



Published in final edited form as:

*Int J Biochem Cell Biol.* 2016 October ; 79: 360–369. doi:10.1016/j.biocel.2016.09.002.

## Curcumin-Loaded Embryonic Stem Cell Exosomes Restored Neurovascular Unit Following Ischemia-Reperfusion Injury

Anuradha Kalani<sup>1,\*</sup>, Pankaj Chaturvedi<sup>1</sup>, Pradip K. Kamat<sup>1</sup>, Claudio Maldonado<sup>1,2</sup>, Philip Bauer<sup>2</sup>, Irving G. Joshua<sup>1</sup>, Suresh C. Tyagi<sup>1</sup>, and Neetu Tyagi<sup>1</sup>

<sup>1</sup>Department of Physiology, School of Medicine, University of Louisville, KY, USA

<sup>2</sup>Department of Surgery, University of Louisville, KY, USA

### Abstract

We tested whether the combined nano-formulation, prepared with curcumin (anti-inflammatory and neuroprotective molecule) and embryonic stem cell exosomes (*MESC-exo<sup>cur</sup>*), restored neurovascular loss following an ischemia reperfusion (IR) injury in mice. IR-injury was created in 8–10 weeks old mice and divided into two groups. Out of two IR-injured groups, one group received intranasal administration of *MESC-exo<sup>cur</sup>* for 7 days. Similarly, two sham groups were made and one group received *MESC-exo<sup>cur</sup>* treatment. The study determined *MESC-exo<sup>cur</sup>* reduced neurological score, infarct volume and edema following IR-injury. As compared to untreated IR group, *MESC-exo<sup>cur</sup>* treated-IR group showed reduced inflammation and N-methyl-D-aspartate receptor expression. Treatment of *MESC-exo<sup>cur</sup>* also reduced astrocytic GFAP expression and alleviated the expression of NeuN positive neurons in IR-injured mice. In addition, *MESC-exo<sup>cur</sup>* treatment restored vascular endothelial tight (claudin-5 and occludin) and adherent (VE-cadherin) junction proteins in IR-injured mice as compared to untreated IR-injured mice. These results suggest that combining the potentials of embryonic stem cell exosomes and curcumin can help neurovascular restoration following ischemia-reperfusion injury in mice.

### Keywords

Curcumin; Exosomes; Neurons; Stroke

### Introduction

According to the recent reports, stroke is the fifth major cause of death and a leading cause of disability in adults of United States (Kochanek et al., 2014; Mozaffarian et al., 2015). Each year about 800,000 US people experience stroke and on average, one American death was reported every 4 min (Mozaffarian et al., 2015). After attempting decades of efforts in developing neuro-restoration therapy that could also help reducing ischemic lesion volume,

\*Correspondence Address: Anuradha Kalani, MS, PhD, Department of Physiology, 500, South Preston Street, Health Sciences Centre, 1201, University of Louisville, Louisville, KY, 40202, Tel: 1-(502)-852-6309, a0kala02@louisville.edu.

**Publisher's Disclaimer:** This is a PDF file of an unedited manuscript that has been accepted for publication. As a service to our customers we are providing this early version of the manuscript. The manuscript will undergo copyediting, typesetting, and review of the resulting proof before it is published in its final citable form. Please note that during the production process errors may be discovered which could affect the content, and all legal disclaimers that apply to the journal pertain.

only thrombolytic therapy had shown beneficiary effects (Li et al., 2014). However, there remains always a need for powerful and innovative therapy that can limit cascades of ischemia and associated pathology.

Exosomes are the secretory nano-vesicles (<200 nm) that recently acquired great scientific attention because of their ability to transfer cellular and biological information, serving as biomarkers and their potential role in therapeutics (Kalani et al., 2014d; Kalani and Tyagi, 2015). Exosomes possess intrinsic ability to cross blood-brain barrier (BBB) and hence, suitable to overcome the problems associated with powerful and potential drugs that cannot reach to clinical trials because of their BBB impermeability (Pardridge, 2012). Of most interest, exosomes possess paracrine properties, special cargos of miRNA, mRNA, proteins and lipids, of the cell type from where they release (Gangoda et al., 2015; Zhang and Grizzle, 2014). In this regard, stem cell derived exosomes have been studied to possess enormous rejuvenating powers that can reprogram the target cell to augment the repair/regeneration processes (Khan et al., 2015; Lai et al., 2012). Stem cell-derived exosomes not only found equally beneficial as stem cells but can also overcome limitations associated with cell-based therapy at ischemic area (Khan et al., 2015). A large body of evidences suggests mesenchymal stem cell (MSC) derived exosomes possess a myriad of beneficiary effects against stroke by promoting functional recovery, neurovascular plasticity, neuroprotection, neuroregeneration and modulating peripheral post-stroke immune responses (Doeppner et al., 2015; Xin et al., 2013). The therapeutic power of MSC-derived exosomes was proposed by transferring functional miRNAs to the recipient cells (Chopp and Zhang, 2015; Xin et al., 2012). Recently embryonic stem cell-derived exosomes have been found to promote endogenous repair mechanisms and enhancing cardiac functions following myocardial infarction (Khan et al., 2015). The same study reported enrichment of embryonic stem cell-specific miRNAs in the exosomes population derived from embryonic-stem cells (Khan et al., 2015). However, there is lack of reports that suggest the therapeutic efficacy of embryonic stem cell-derived exosomes against ischemic stroke.

Curcumin, a natural polyphenol found in the rhizomes of *Curcuma longa* (turmeric), is yellow colored spice and possess remarkable medicinal properties. The therapeutic efficacy of curcumin has been extensively studied against ischemic stroke which is attributed by promoting free radical scavenging, anti-inflammatory, anti-lipidemic and anti-aggregation properties (Kalani et al., 2014c; Soni and Kuttan, 1992; Strimpakos and Sharma, 2008). Extensive medicinal properties led curcumin towards clinical trials to prevent brain diseases; however, phase-I clinical trials were unsuccessful because of its low bioavailability (Anand et al., 2007; Ovbiagele, 2008; Perry and Howes, 2011). Poor absorption, quick metabolism, and rapid systemic elimination are the factors that limit curcumin bioavailability. These problems led other ways explored by the investigators. Patra et. al. (Patra and Sleem, 2013) have developed a novel method for encapsulation of curcumin by synthesizing microcapsule containing self-assembled nanoparticles using poly (L-lysine), trisodium citrate and silica sol. Mouslmani et al (Mouslmani M, 2015) developed hierarchically ordered nanocapsule structures by crosslinking curcumin associated poly (allylamine hydrochloride) with dipotassium phosphate and subsequently congregates with silica nanoparticles (Mouslmani M, 2015). Excitingly, curcumin loaded in exosomes was not only found more stable, highly soluble and highly concentrated in the blood but also appeared to express more therapeutic

potentials (Sun et al., 2010; Zhuang et al., 2011). In the current report, we sought to determine the neuro-vascular restoration therapy of *MESC-exo<sup>cur</sup>* [curcumin loaded in *MESC-exo* (mouse embryonic stem cell-derived exosomes)] following an ischemia reperfusion injury in mouse model.

## Methodology

All procedures were conducted in compliance with guidelines established by the National Institute of Health (NIH) Guide for the Care and Use of Laboratory Animals and were approved by the University of Louisville's Institutional Animal Care and Use Committee. 8–10 weeks old male wild-type (WT, C57BL/6J) mice were obtained from the Jackson Laboratory (Bar Harbor, ME, USA). The experimental mice groups were: 1) sham, 2) sham + *MESC-exo<sup>cur</sup>*, 3) IR, and 4) IR+ *MESC-exo<sup>cur</sup>*.

### Animal Surgical Procedure

Mice were anesthetized with sodium pentobarbital (50 mg/kg body wt.) and operated within 1h. Anesthetized mice were orally intubated, mechanically ventilated and the body temperature was maintained at  $37 \pm 1^\circ\text{C}$  during surgery. A midline neck incision was made and common carotid artery (CCA) was exposed carefully. Silicon-rubber coated monofilament (diameter 0.22, 0.23 mm, size 6-0 or 7-0) was used to obstruct middle cerebral artery after inserting it into internal carotid artery and advancing to internal carotid artery. After 40 min of surgery, the filaments were withdrawn to allow reperfusion. Same anesthesia and surgical procedures were performed in sham groups of mice except the insertion of monofilament (Kalani et al., 2015). After the surgery, mice were tested for the neurobehavioral tests to determine neurological deficit score (Belayev et al., 1996; Kalani et al., 2015). The neurological deficit score was reported on a blind fashion using a scale 0 to 12 (normal score=0, maximum=12). Mice showing high neurological deficit scores (>10) were used in the current study.

### Isolation of mouse embryonic stem cell exosomes and their characterization

Mouse embryonic stem cell line was procured from American Type Culture Collection (ATCC, Menassas, VA, USA) and grown on a fibroblast monolayer as per supplier's step-by-step protocol. The cells were maintained in 25 or 75 cm<sup>2</sup> tissue culture flasks under the atmosphere set at 5% CO<sub>2</sub> and 95% air in an incubator. For exosome collection, the cells were made 50–60% confluent and the media was changed, which was prepared with exosome free serum. After 48–72 h of culture, media was collected and processed as described in our earlier report (Kalani et al., 2014a), with certain modifications. Briefly, culture media was centrifuged at  $3,000 \times g$  (10 min) and supernatant was re-centrifuged at  $10,000 \times g$  (15 min).  $10,000 \times g$  supernatant was collected and ultracentrifuged at  $1,40,000 \times g$  for 3 h to concentrate *MESC-exo* in pellet. Characterization of exosome was performed with western blot with TSG101 antibody (Kalani et al., 2014a), acetylcholinesterase activity (Kalani et al., 2014a), and nano-tracking (NTA) analysis (Sokolova et al., 2011).

### Packing of curcumin in MESC-exo and intranasal delivery

The loading of curcumin (dissolved in ethanol) was achieved by mixing it to *MESC-exos* in a fixed proportion (1: 4). The nanopreparation was incubated for 15 min at room temperature and rapid freeze-thawing was done 2–3 times. The unbound drug was removed by centrifuging the preparation twice at 5,000 Xg. The formulation was precipitated either by ultracentrifuging at 1, 40,000 × g for 3 h or precipitating with total exosome isolation reagent (ThermoFisher Scientific, Grand Island, NY, USA). Fresh preparations of *MESC-exo<sup>cur</sup>* were used for intranasal delivery in two groups of mice (sham + *MESC-exo<sup>cur</sup>* and IR + *MESC-exo<sup>cur</sup>*). Total 10 µl *MESC-exo<sup>cur</sup>* was administered, twice a day, by alternate nostrils (2 µl × 5 times) started within an hour of IR and sham surgery and continued till 7 days. Neurological behavior tests for instance, posture relax test, forelimb placing test and motor coordination tests were performed on 1<sup>st</sup>, 3<sup>rd</sup> and 7<sup>th</sup> day post- *MESC-exo<sup>cur</sup>* administration.

### Collection of brain samples

At the end of the experiment, mice were intracardially perfused with phosphate buffer saline (50mM PBS, pH=7.4) under deep anesthesia. Brain samples were carefully harvested after opening the cranium, washed with ice-cold PBS, and used for various experimental procedures.

### Determination of Infarct Volume (IV)

2 mm size coronal sections were cut using a mouse brain slice matrix (Harvard Apparatus, Holliston, MA, USA). 2% of 2,3,5-Triphenyltetrazolium chloride (TTC; Sigma Aldrich, Taufkirchen, Germany) was used to stain the sections. After staining the sections for 20 min in TTC, sections were fixed in 4% paraformaldehyde. Infarct area (pale white color) was determined with image analysis software (Image-Pro Plus, USA).

### Cerebral edema

The cortical parts of the brain ipsilateral area were dried for 3 days in drying oven at 100°C. Water content was calculated in percentage using the formula, (wet weight-dry weight)/wet weight]\*100.

### Measurement of reactive oxygen species (ROS)

The ROS level was determined in the experimental brains spectrometrically as determined earlier (Tota et al., 2012). Briefly, brain tissue was minced and treated with collagenase (750 unit/ml) in HEPES–Tyrode solution (145 mM NaCl, 5 mM KCl, 2 mM CaCl<sub>2</sub>, 1 mM MgCl<sub>2</sub>, 5 mM glucose, 5 mM HEPES, pH 7.4) for 40 min at 37°C. Dissociated cells were stained with oxidation sensitive fluorescent probe 5 µM DCF (2',7'-dichlorodihydrofluorescein diacetate) for 15 min at 37°C and then washed with HEPES. The formation of the fluorescent product DCF was assessed with excitation/emission wavelengths of 488 nm/530 nm.

### Measurement of Lipid Peroxidation

Malondialdehyde (MDA), one of the final products of polyunsaturated fatty acids peroxidation, was used to assess lipid peroxidation using 1,1,3,3-tetraethoxypropane as a standard. Cerebral cortex and hippocampus regions of the mice brains were homogenized and tested separately. The reaction mixture was consisted of 0.3 ml thiobarbituric acid (2 %), and 0.15 ml 5 N HCl with homogenized brain tissue samples (Kalani et al., 2014b). The samples were shaken well and heated at 90 °C for 15 min. After centrifuging the mixture at 13,000 rpm for 10 min, the pink-colored supernatant was collected and absorbance was measured at 532 nm using a Spectra Max M2 plate reader (Molecular Device, Sunnyvale, CA, USA).

### Measurement of Glutathione

DTNB (5,5'-dithiobis 2-nitrobenzoic acid) was used to ascertain glutathione (GSH) level as described previously (Kalani et al., 2014b). Briefly, homogenized cortical and hippocampus samples were treated with an equal volume of 5 % TCA and centrifuged at 3,000 rpm for 10 min. The supernatant (0.05 ml) was transferred to another tube containing 0.1 ml phosphate buffer (pH 8.4), DTNB, and 0.05 ml double distilled water. The content of the tube were mixed and absorbance was recorded at 412 nm using a Spectra Max M2 plate reader (Molecular Device).

### SDS-PAGE and Western Blotting

Protein from brain sample was extracted in radioimmumoprecipitation assay (RIPA) buffer (50 mM Tris-HCl, pH 7.4; 1% NP-40; 0.25% Na-deoxycholate, 150 mM NaCl; 1 mM EDTA; 1 µg/ml each of aprotinin, leupeptin, pepstatin; 1 mM Na<sub>3</sub>VO<sub>4</sub>; 1 mM NaF) containing protease inhibitors (1 mM phenylmethanesulfonyl fluoride and 1 µg complete protease inhibitors, Sigma). Supernatant was collected after centrifuging the brain homogenate at 12,000 × g for 15 min in cold condition. Protein estimation of the samples was performed using Bradford reagent (BioRad, CA, USA) against a bovine serum albumin standard (BSA) (Kalani et al., 2014b). Equal quantity (25 µg) of protein samples from different experimental groups were run on SDS-PAGE. The separated proteins on the gel were transferred to polyvinyl difluoride (PVDF) membrane by using an electrotransfer apparatus (Bio-Rad). The transfer was run overnight at 120 mA in cold condition. The membrane was checked with ponceau dye (BioRad) to ensure the transfer and processed for blocking with 5% non-fat dry milk in PBS. After that, membrane was incubated overnight in primary antibody (GFAP, dilution 1:500) at 4°C. After washing unbound antibody, membrane was incubated with appropriate secondary antibody (Santa cruz, dilution 1:5000) at room temperature for 60 min and developed with chemiluminescent developing reagent (Biorad). The membrane was stripped and re-probed with anti-GAPDH antibody (Millipore, dilution 1:1000), which was used as a loading control. The images were acquired in a gel documentation system (BioRad) and densitometry analysis was performed using the image lab software.

## Quantitative gene expression analysis

Total RNA from experimental brain tissues were isolated using TRIzol® reagent (Invitrogen, Grand Island, NY, USA) as per manufacture's protocol. The pure quality and quantity of RNA was confirmed by using nanodrop-1000 (Thermo Scientific, Waltham, MA, USA). Complimentary DNA (cDNA) was prepared from RNA using manufacture's protocol (Im-Prom-II™, Invitrogen, USA). CDNA samples were amplified for the given genes by gene-specific primers (TNF- $\alpha$ , NMDA-R1, NR2A, NR2B and Rn18s or GAPDH) using Stratagene Mx3000p (Agilent Technologies, Santa Clara, CA, USA). After baseline and threshold adjustments, CT (cycle threshold) values were determined. The transcript levels of given genes were normalized with Rn18s/GAPDH and the data was expressed in fold expression.

## Immunohistochemistry

For a set of experiments, mice were infused with tetramethylrhodamine  $\beta$ -isothiocyanate (TRITC) - conjugated lycopersicon esculentum agglutinin (LEA) tomato lectin (Vector Laboratories, Burlingame, CA, USA) through carotid artery cannulation. LEA binds to vascular endothelial cells. Animals were perfused transcardially with PBS under anesthetic overdose. Cranium was carefully opened and the brain was gently removed. Frozen brain blocks (prepared with OCT media, Triangle Biomedical Sciences, Durham, NC, USA) were prepared and 15 $\mu$ m coronal brain sections were cut using a cryostat (Leica CM, USA).

For other sets of experiments, frozen blocks were cut into 25  $\mu$ m sections using a cryostat. The sections were post-fixed after removing mounting matrix and then blocked with blocking solution (0.1% Triton X-100 TBS (TBS-T), 0.5% BSA, and 10% normal donkey serum) for 1 h at room temperature. Sections were incubated overnight in primary antibody for ICAM (Santa cruz, 1: 100), GFAP (Neuromab, 1: 100), NeuN (Abcam, 1:200), VE-cadherin (Santa cruz, 1: 100), claudin-5 (Santa cruz, 1:200), occludin (Santa cruz, 1: 100) at 4°C. After washing the unbound antibody in TBS, the sections were further incubated with appropriate fluorescence secondary antibodies for 60 min at room temperature. After that, sections were incubated with DAPI (1:10,000) for 10 min at room temperature and mounted with anti-fade mounting media. Images were acquired using a laser scanning confocal microscope (FluoView 1000; Olympus, PA, USA) and the data was analyzed with image analysis software (Image-Pro Plus; Media Cybernetics, Rockville, MD, USA).

## Statistical Analysis

All values are expressed as mean  $\pm$  SEM. Interaction between groups was determined by one-way analysis of variance (ANOVA) test followed by appropriate post-hoc test. P value equal to or less than 0.05 was considered statistically significant.

## RESULTS

### 1. Isolation of MESC-exo and characterization of MESC-exo<sup>cur</sup>

Based on the Brownian motions, the size of the *MESC-exo* was determined as 118 nm by NTA (Figure-1A, 1B, 1C). The integrity of *MESC-exo* and *MESC-exo*<sup>cur</sup> (curcumin loaded in *MESC-exo*) was determined by Western blotting with TSG101 antibody and AchE

activity. Western blot analysis determined specific presence of TSG101 band in *MESC-exo<sup>cur</sup>* and *MESC-exo* preparations (Figure-1D). The two preparations (*MESC-exo<sup>cur</sup>* and *MESC-exo*) also showed greater AchE activity as compared to control (culture condition media supernatant deprived of exosomes; 1, 40,000 × g supernatant) (Figure-1E).

## 2. *MESC-exo<sup>cur</sup>* treatment reduced post ischemic events in Ischemia injured IR mice

We determined whether intranasal delivery targets *MESC-exo<sup>cur</sup>* units to the brain using IHC analysis of the brain coronal sections. Mice administered intra-nasally with fluorescent *MESC-exo<sup>cur</sup>* showed presence of *MESC-exo<sup>cur</sup>* in different brain cellular compartments; astrocytes (GFAP), neurons (NeuN), and vessels (LEA) (Figure-2A).

To determine the therapeutic efficacy of *MESC-exo<sup>cur</sup>* against IR-injury, we determined neurological score, lesion volume, and cerebral edema in IR-injured mice. As compared to IR mice, IR+ *MESC-exo<sup>cur</sup>* mice showed improvement in neurological scores at 3<sup>rd</sup> and 7<sup>th</sup> day after treatment (Figure-2B). Similarly, *MESC-exo<sup>cur</sup>* administered IR-mice showed significant reduction in lesion volume, and brain water content as compared to untreated IR-mice (Figure-2C, 2D). No considerable signs of neurological deficits, brain water content and injured volume were detected in sham and sham+ *MESC-exo<sup>cur</sup>* mice (Figure-2B, 2C, 2D).

## 3. *MESC-exo<sup>cur</sup>* treatment reduced inflammation

Since inflammation mediates myriads of pathological events following an ischemic insult, we determined whether *MESC-exo<sup>cur</sup>* can reduce inflammation which further decreases reactive oxygen species. IR-injured mice showed increased level of ROS, which got significantly decreased with *MESC-exo<sup>cur</sup>* treatment (Figure-3A). Through real-time PCR analysis, we determined the transcript expression of an important pro-inflammatory cytokine, TNF- $\alpha$ , in different experimental mice groups. IR mice showed high TNF- $\alpha$  mRNA levels which got significantly reduced in IR+ *MESC-exo<sup>cur</sup>* mice (Figure-3B). Considerable change in TNF- $\alpha$  mRNA level was not observed in sham+ *MESC-exo<sup>cur</sup>* mice, as compared to sham (Figure-3B). As pro-inflammatory cytokines mediate molecular pathways for the inductions of NMDARs, we determined the beneficiary effects of *MESC-exo<sup>cur</sup>* that could help reducing NMDARs. IR mice showed increased NR1 mRNA expression, and decreased NR2A and NR2B mRNA expressions. Treatment of *MESC-exo<sup>cur</sup>* significantly downregulated NR1 mRNA level in IR mice, however; no changes in NR2A and NR2B mRNA levels were observed in IR+ *MESC-exo<sup>cur</sup>* mice (Figure-3C). Alongside, no changes in different NMDARs levels were found in sham+ *MESC-exo<sup>cur</sup>* mice as compared to sham (Figure-3C). IR mice also showed high malondialdehyde(MDA) and reduced glutathione (GSH) levels in cerebral cortex and hippocampus regions, as compared to sham group. Treatment of *MESC-exo<sup>cur</sup>* reduced MDA and improved GSH level in the two brain regions of IR mice (table-1)

## 4. *MESC-exo<sup>cur</sup>* treatment normalized astrocytes and neuronal expression

Ischemic brain pathology mediates through astrogliosis that can further affect neuronal functions. In this regard, we determined the therapeutic effects of *MESC-exo<sup>cur</sup>* in normalizing astrogliosis and saving neurons. IHC analysis of IR mice brain showed induced

GFAP expression around vascular (Figure-4A) and cortical area (Figure-4B). On contrary, significantly reduced NeuN positive neurons were observed around vascular (Figure-4A) and cortical area in IR mice (Figure-4B). *MESC-exo<sup>cur</sup>* treatment in IR mice not only considerably reduced GFAP expression but also rescued NeuN positive neurons to a significant extent (Figure-4A, 4B, 4C). No alterations in GFAP positive astrocytes and NeuN positive neurons, around vascular and cortical areas, were observed in sham + *MESC-exo<sup>cur</sup>* mice as compared to sham (Figure-4A, 4B, 4C). Western blot analysis also revealed induced expression of GFAP in IR-injured mice brain (Figure-4D, 4E). Treatment with *MESC-exo<sup>cur</sup>* reduced GFAP to a considerable extent in IR-injured mice (Figure-4D, 4E).

### 5. *MESC-exo<sup>cur</sup>* treatment mitigated vascular ICAM and endothelial junction protein expressions

We next determined the beneficiary effects of *MESC-exo<sup>cur</sup>* in reducing vascular inflammation (ICAM) and improving endothelial vascular junction protein (VE-cadherin). IHC analysis showed significant increase in ICAM levels and reduction in VE-cadherin level in brain vessels of IR mice (Figure-5A, 5B). As compared to IR mice, IR+ *MESC-exo<sup>cur</sup>* mice showed notable reduction in ICAM and improvement in VE-cadherin levels in brain vessels (Figure-5A, 5B). However, no change in ICAM and VE-cadherin was observed in sham+ *MESC-exo<sup>cur</sup>* mice as compared to sham (Figure-5A, 5B).

### 6. *MESC-exo<sup>cur</sup>* treatment reduced tight junction proteins loss

The breakdown of vascular junction proteins can intensify the stroke intensity, therefore; we determined the expressions of vascular tight junction proteins, claudin-5 and occludin. IR mice vessels showed reduced expressions of claudin-5 and occludin which were considerably improved after treating IR mice with *MESC-exo<sup>cur</sup>*. Sham and sham+ *MESC-exo<sup>cur</sup>* mice groups did not show any considerable changes in claudin-5 and occludin expressions.

## Discussion

In the current report, we determined the therapeutic potentials of curcumin-loaded embryonic stem cell exosomes (*MESC-exo<sup>cur</sup>*) in neurovascular restoration following IR-injury in mice. Our results indicate that *MESC-exo<sup>cur</sup>* reduced neurological score, infarct volume, edema, inflammation, astrogliosis, and NMDAR1 expression following IR-injury in mice. In addition, treatment of *MESC-exo<sup>cur</sup>* restored NeuN positive neurons, reduced vascular inflammation and alleviated tight and adherent junctions following IR-injury in mice.

In *MESC-exo<sup>cur</sup>* units, there were two therapeutic components: 1, embryonic stem cell derived-exosomes that contain enormous paracrine factors of stem cells; and 2, curcumin, a potent therapeutic molecule. The ability of exosome and curcumin to cross BBB also increases their chance to use as cerebral therapies (Kalani et al., 2014c; Kalani et al., 2014d; Kalani and Tyagi, 2015; Mishra and Palanivelu, 2008). Recently, stem cell exosomes have been shown therapeutic potentials following stroke (Doepfner et al., 2015; Khan et al., 2015; Xin et al., 2013). Curcumin possesses a potent anti-inflammatory and anti-oxidative

properties and its role in ischemic injury has been largely studied (Dai et al., 2015; Ji et al., 2014; Li et al., 2015; Thiyagarajan and Sharma, 2004). Low bioavailability due to poor absorption, rapid systemic elimination and quick metabolism limit therapeutic efficacy of curcumin to a significant extent (Kalani et al., 2014c). Exosomes have been found potential sources that can naturally carry and deliver curcumin (Fan et al., 2014). Curcumin loaded on exosomes was found to be more soluble, stable and bioavailable and thus showed enhance anti-inflammatory activity against lipopolysaccharide induced septic shock mouse model (Fan et al., 2014). In agreement, we also found more solubility and stability of curcumin in our exosomal nano-formulations *MESC-exo<sup>cur</sup>* (data not shown). In addition, a recent study determined 10–40% drug (chemopreventive, chemotherapeutic, and curcumin) load in exosomes derived from bovine milk (Munagala et al., 2015). Using AchE and western blotting analysis, with exosome specific antibody TSG101, we found that *MESC-exo<sup>cur</sup>* units showed AchE activity and specific TSG101 band similar to *MESC-exo*. These results clearly indicate that the integrity of exosomes was preserved while loading curcumin to exosomes. We used intranasal delivery of *MESC-exo<sup>cur</sup>* that showed successful cerebral delivery and neurovascular restorations following an IR-injury. Earlier, intranasal deliveries of curcumin and catalase loaded-exosomes were also found to get targeted to the brain and effective against LPS-induced brain inflammation and Parkinson's disease mice models (Haney et al., 2015; Zhuang et al., 2011). Although the exact route from nasal route to the brain is not cleared, the transport is believed to be mediated through olfactory and trigeminal nerves (Zhuang et al., 2011). We reported the presence of exosomes to different cellular components of the mouse brain after intranasal administration, for instance; glia, neurons and around vascular endothelial cells, which is in consistent with previous reports (Haney et al., 2015; Zhuang et al., 2011). The choice of *MESC-exo<sup>cur</sup>* administration through intranasal route in IR-injured mice was based on exciting findings of the previous study (Zhuang et al., 2011). In the later study curcumin-loaded exosomes, administered through intranasal route, were detectable till 12 h in olfactory bulb and repeated administration of exosome loaded curcumin maintained the curcumin concentration at an average of  $2.6 \pm 0.4$  nmol/g of brain tissue (Zhuang et al., 2011). Wang et al. (Wang et al., 2012) have also reported that the distribution of curcumin in brain versus blood was found higher through intranasal route as compared to other routes. As compared to untreated IR-injured mice, *MESC-exo<sup>cur</sup>*-treated mice showed significant decrease in neurological score starting from 3<sup>rd</sup> day of treatment. Notable decrease in cerebral edema and infarct volume was also noticed in *MESC-exo<sup>cur</sup>*-treated mice that suggests therapeutic potential of exosomal nano-formulations.

Inflammatory mechanisms are responsible for several brain-associated pathologies and injuries, including IR-injury (Lakhan et al., 2009; Rai et al., 2013). The injured tissue following IR-injury releases the ROS that triggers the inflammatory cytokine levels. We reported increased ROS and pro-inflammatory cytokine TNF- $\alpha$  levels increased in IR injured brain; however, consistent treatment of *MESC-exo<sup>cur</sup>* for 7 days extensively reduced the levels of pro-inflammatory cytokine TNF- $\alpha$  level, and ROS. Potent anti-inflammatory effects of curcumin and its increased bioavailability helped in decreasing IR-induced ROS and inflammation. NMDA receptors (NMDARs), the glutamate receptors, are of major interest as they are involved in synaptogenesis, synaptic plasticity, and neuronal circuitry

formation. Overactivity of NMDARs results in excitotoxicity that may activate microglia (Chang et al., 2008). In addition to presence of NMDARs in neuronal population, a report suggests the presence of NMDARs in development, ischemia and post-ischemic events (Zhou et al., 2010). The studies on animal subjects clearly indicate the involvement of astrocytic glutamate receptor in glial cell signaling (Schipke et al., 2001; Wong, 2006). In our study, although we observed alterations in NR1, NR2A and NR2B transcripts following IR-insult in mice; however, only NR1 levels were recovered to a significant extent with the use of *MESC-exo<sup>cur</sup>*. This suggests the importance of NR1 in restoring neurological events following IR-injury, as studied earlier (Wang et al., 2013). Astrogliosis, reactive astrocytes, is a process of abnormal increase of astrocytic population after an injury (Gordon et al., 2007). Reactive astrocytes can benefit or harm neuronal and non-neuronal system they interact. Though not studied in detail, astrocytes have been found to release TNF- $\alpha$  and other inflammatory cytokine levels after a scratch and ischemic injury (Lau and Yu, 2001). We determined increased GFAP activity, a marker of reactive astrocytes, as well as increased TNF- $\alpha$  expression in IR-injured brain. In addition, the neuronal marker NeuN immunoreactivity was decreased in ischemic lesion suggesting neuronal loss after IR-injury. The use of *MESC-exo<sup>cur</sup>* not only helped in restoration of NeuN positive neurons but also in reducing astrogliosis as determined by decreased GFAP expression in IR-injured mice brains.

In addition to neuro-glial system, the therapeutic role of *MESC-exo<sup>cur</sup>* was also studied against IR-injured vascular impairment. ICAM-1, a marker of vascular inflammation, expression increases in the presence of pro-inflammatory cytokines, which is otherwise reported low at the basal level (Huber et al., 2006). The interaction of induced ICAM-1 with disrupted BBB was studied in atherosclerosis, inflammation, and thrombosis (Corti et al., 2004). The BBB integrity is critically maintained with endothelial tight and adherens junction proteins (Kalani et al., 2014b; Kalani et al., 2015). IR-injury decreases endothelial junction proteins which also progresses under enhanced inflammation (Kalani et al., 2015). Similar to these studies, we also found induced ICAM-1 expression and reduced tight junctions (claudin-5 and occludin) and adherent junction (VE-cadherin). The use of *MESC-exo<sup>cur</sup>* restored considerable vascular integrity by reducing vascular inflammation and restoring tight and adherens junction proteins. Although the findings of the study are exciting that can help in future powerful therapy development, there are certain limitations of the study. First, the treatment of IR-injured mice was started within an hour of injury which does not clinically implicate the conditions of the stroke patients who sometimes reach to the hospitals after hours of ischemic insult. Second, the lack of additional mice groups treated with curcumin and embryonic stem cells alone to compare the combined *MESC-exo<sup>cur</sup>* effects. Third, time points analysis of available curcumin concentrations in the blood and mice brain tissues. Hence, future studies are warranted to overcome the given and other relevant limitations associated with the study.

In conclusion, we designed a combined powerful formulation by combining embryonic stem cell exosomes and curcumin, *MESC-exo<sup>cur</sup>*, to treat IR-injury in mice. The study results suggest that the innovative formulation helped in restoration of neuro-glial-vascular losses following IR-injury. Exciting results with the nano-formulation and intranasal delivery of

*MESC-exo<sup>cur</sup>* provides the hope for future potential and non-invasive therapeutics for stroke. The hypothesis is presented in pictorial presentation (Figure-7).

## Acknowledgments

Part of this study was supported by NIH grants HL-074185 and HL-107640 to SCT and NT. PC was supported by a post-doctoral grant from American Heart Association, 15POST23110021.

## Abbreviations

<b>AchE</b>	Acetylcholinestrase
<b>BBB</b>	Blood brain barrier
<b>BSA</b>	Bovine serum albumin
<b>cDNA</b>	Complimentary DNA
<b>DAPI</b>	4,6-diamidino-2-phenyl-indole HCl
<b>FIU</b>	Fluorescence intensity units
<b>GAPDH</b>	Glyceraldehyde-3-phosphate dehydrogenase
<b>GFAP</b>	Glial fibrillary acidic protein
<b>ICAM</b>	Intra cellular adhesion molecule-1
<b>IHC</b>	Immunohistochemistry
<b>IR</b>	Ischemia Reperfusion
<b>LEA</b>	Lycopersicon Esculentum agglutinin tomato lectin
<b>LPS</b>	Lipopolysaccharide
<b><i>MESC-exo</i></b>	Mouse embryonic stem cell exosomes
<b><i>MESC-exo<sup>cur</sup></i></b>	Curcumin loaded mouse embryonic stem cell exosomes
<b>NeuN</b>	Neuronal nuclei
<b>NMDARs</b>	N-methyl-D-aspartate receptors
<b>NTA</b>	Nanoparticle tracking analysis
<b>PBS</b>	Phosphate buffer saline
<b>QPCR</b>	Quantitative PCR
<b>RIPA</b>	Radioimmunoprecipitation assay buffer
<b>ROS</b>	Reactive oxygen speies
<b>TBS</b>	Tris-buffered saline

<b>TBS-T</b>	Tris-buffered saline with Triton X-100
<b>TNF-<math>\alpha</math></b>	Tumor necrosis factor
<b>TSG101</b>	Tumor susceptibility gene101

## References

- Anand P, Kunnumakkara AB, Newman RA, Aggarwal BB. Bioavailability of curcumin: problems and promises. *Mol Pharm.* 2007; 4(6):807–818. [PubMed: 17999464]
- Belayev L, Alonso OF, Busto R, Zhao W, Ginsberg MD. Middle cerebral artery occlusion in the rat by intraluminal suture. Neurological and pathological evaluation of an improved model. *Stroke.* 1996; 27(9):1616–1622. discussion 1623. [PubMed: 8784138]
- Chang YC, Kim HW, Rapoport SI, Rao JS. Chronic NMDA administration increases neuroinflammatory markers in rat frontal cortex: cross-talk between excitotoxicity and neuroinflammation. *Neurochem Res.* 2008; 33(11):2318–2323. [PubMed: 18500552]
- Chopp M, Zhang ZG. Emerging potential of exosomes and noncoding microRNAs for the treatment of neurological injury/diseases. *Expert Opin Emerg Drugs.* 2015; 20(4):523–526. [PubMed: 26135408]
- Corti R, Hutter R, Badimon JJ, Fuster V. Evolving concepts in the triad of atherosclerosis, inflammation and thrombosis. *J Thromb Thrombolysis.* 2004; 17(1):35–44. [PubMed: 15277786]
- Dai LY, Cheng BH, Li J. Effect of Curcumin on Cerebral Ischemia-reperfusion Injury in Rats. *Zhong Yao Cai.* 2015; 38(2):344–349. [PubMed: 26415414]
- Doepfner TR, Herz J, Gorgens A, Schlechter J, Ludwig AK, Radtke S, de Miroschedji K, Horn PA, Giebel B, Hermann DM. Extracellular Vesicles Improve Post-Stroke Neuroregeneration and Prevent Postischemic Immunosuppression. *Stem Cells Transl Med.* 2015; 4(10):1131–1143. [PubMed: 26339036]
- Fan X, Jiang Y, Yu Z, Yuan J, Sun X, Xiang S, Lo EH, Wang X. Combination approaches to attenuate hemorrhagic transformation after tPA thrombolytic therapy in patients with poststroke hyperglycemia/diabetes. *Adv Pharmacol.* 2014; 71:391–410. [PubMed: 25307224]
- Gangoda L, Boukouris S, Liem M, Kalra H, Mathivanan S. Extracellular vesicles including exosomes are mediators of signal transduction: are they protective or pathogenic? *Proteomics.* 2015; 15(2–3): 260–271. [PubMed: 25307053]
- Gordon GR, Mulligan SJ, MacVicar BA. Astrocyte control of the cerebrovasculature. *Glia.* 2007; 55(12):1214–1221. [PubMed: 17659528]
- Haney MJ, Klyachko NL, Zhao Y, Gupta R, Plotnikova EG, He Z, Patel T, Piroyan A, Sokolsky M, Kabanov AV, Batrakova EV. Exosomes as drug delivery vehicles for Parkinson's disease therapy. *J Control Release.* 2015; 207:18–30. [PubMed: 25836593]
- Huber JD, Campos CR, Mark KS, Davis TP. Alterations in blood-brain barrier ICAM-1 expression and brain microglial activation after lambda-carrageenan-induced inflammatory pain. *Am J Physiol Heart Circ Physiol.* 2006; 290(2):H732–740. [PubMed: 16199477]
- Ji B, Han Y, Liu Q, Liu X, Yang F, Zhou R, Lian Q, Cao H, Li J. Curcumin improves the impaired working memory in cerebral ischemia-reperfusion rats by inhibiting proinflammatory cytokines. *Zhonghua Yi Xue Za Zhi.* 2014; 94(13):1029–1033. [PubMed: 24851695]
- Kalani A, Kamat PK, Chaturvedi P, Tyagi SC, Tyagi N. Curcumin-primed exosomes mitigate endothelial cell dysfunction during hyperhomocysteinemia. *Life Sci.* 2014a; 107(1–2):1–7. [PubMed: 24780320]
- Kalani A, Kamat PK, Givvimani S, Brown K, Metreveli N, Tyagi SC, Tyagi N. Nutri-epigenetics ameliorates blood-brain barrier damage and neurodegeneration in hyperhomocysteinemia: role of folic acid. *J Mol Neurosci.* 2014b; 52(2):202–215. [PubMed: 24122186]
- Kalani A, Kamat PK, Kalani K, Tyagi N. Epigenetic impact of curcumin on stroke prevention. *Metab Brain Dis.* 2014c
- Kalani A, Kamat PK, Tyagi N. Diabetic Stroke Severity: Epigenetic Remodeling and Neuronal, Glial, and Vascular Dysfunction. *Diabetes.* 2015; 64(12):4260–4271. [PubMed: 26470785]

- Kalani A, Tyagi A, Tyagi N. Exosomes: mediators of neurodegeneration, neuroprotection and therapeutics. *Mol Neurobiol*. 2014d; 49(1):590–600. [PubMed: 23999871]
- Kalani A, Tyagi N. Exosomes in neurological disease, neuroprotection, repair and therapeutics: problems and perspectives. *Neural Regen Res*. 2015; 10(10):1565–1567. [PubMed: 26692841]
- Khan M, Nickoloff E, Abramova T, Johnson J, Verma SK, Krishnamurthy P, Mackie AR, Vaughan E, Garikipati VN, Benedict C, Ramirez V, Lambers E, Ito A, Gao E, Misener S, Luongo T, Elrod J, Qin G, Houser SR, Koch WJ, Kishore R. Embryonic stem cell-derived exosomes promote endogenous repair mechanisms and enhance cardiac function following myocardial infarction. *Circ Res*. 2015; 117(1):52–64. [PubMed: 25904597]
- Kochanek KD, Murphy SL, Xu J, Arias E. Mortality in the United States, 2013. *NCHS Data Brief*. 2014; (178):1–8.
- Lai RC, Tan SS, Teh BJ, Sze SK, Arslan F, de Kleijn DP, Choo A, Lim SK. Proteolytic Potential of the MSC Exosome Proteome: Implications for an Exosome-Mediated Delivery of Therapeutic Proteasome. *Int J Proteomics*. 2012; 2012:971907. [PubMed: 22852084]
- Lakhan SE, Kirchgessner A, Hofer M. Inflammatory mechanisms in ischemic stroke: therapeutic approaches. *J Transl Med*. 2009; 7:97. [PubMed: 19919699]
- Lau LT, Yu AC. Astrocytes produce and release interleukin-1, interleukin-6, tumor necrosis factor alpha and interferon-gamma following traumatic and metabolic injury. *J Neurotrauma*. 2001; 18(3):351–359. [PubMed: 11284554]
- Li W, Suwanwela NC, Patumraj S. Curcumin by down regulating NF-kB and elevating Nrf2, reduces brain edema and neurological dysfunction after cerebral I/R. *Microvasc Res*. 2015
- Li Y, Liu Z, Xin H, Chopp M. The role of astrocytes in mediating exogenous cell-based restorative therapy for stroke. *Glia*. 2014; 62(1):1–16. [PubMed: 24272702]
- Mishra S, Palanivelu K. The effect of curcumin (turmeric) on Alzheimer's disease: An overview. *Ann Indian Acad Neurol*. 2008; 11(1):13–19. [PubMed: 19966973]
- Mouslmani M, JMR, Prabhakar Neeraj, Peurla Markus, Baydound Elias, Patra Digambara. Curcumin associated poly(allylamine hydrochloride)-phosphate self-assembled hierarchically ordered nanocapsules: size dependent investigation on release and DPPH scavenging activity of curcumin. *RSC Adv*. 2015; 5:18740–18750.
- Mozaffarian D, Benjamin EJ, Go AS, Arnett DK, Blaha MJ, Cushman M, de Ferranti S, Despres JP, Fullerton HJ, Howard VJ, Huffman MD, Judd SE, Kissela BM, Lackland DT, Lichtman JH, Lisabeth LD, Liu S, Mackey RH, Matchar DB, McGuire DK, Mohler ER 3rd, Moy CS, Muntner P, Mussolino ME, Nasir K, Neumar RW, Nichol G, Palaniappan L, Pandey DK, Reeves MJ, Rodriguez CJ, Sorlie PD, Stein J, Towfighi A, Turan TN, Virani SS, Willey JZ, Woo D, Yeh RW, Turner MB. American Heart Association Statistics C., Stroke Statistics S. Heart disease and stroke statistics--2015 update: a report from the American Heart Association. *Circulation*. 2015; 131(4):e29–322. [PubMed: 25520374]
- Munagala R, Aqil F, Jeyabalan J, Gupta RC. Bovine milk-derived exosomes for drug delivery. *Cancer Lett*. 2015
- Ovbiagele B. Potential role of curcumin in stroke prevention. *Expert Rev Neurother*. 2008; 8(8):1175–1176. [PubMed: 18671659]
- Pardridge WM. Drug transport across the blood-brain barrier. *J Cereb Blood Flow Metab*. 2012; 32(11):1959–1972. [PubMed: 22929442]
- Patra D, Sleem F. A new method for pH triggered curcumin release by applying poly(L-lysine) mediated nanoparticle-congregation. *Analytica chimica acta*. 2013; 795:60–68. [PubMed: 23998538]
- Perry E, Howes MJ. Medicinal plants and dementia therapy: herbal hopes for brain aging? *CNS Neurosci Ther*. 2011; 17(6):683–698. [PubMed: 22070157]
- Rai S, Kamat PK, Nath C, Shukla R. A study on neuroinflammation and NMDA receptor function in STZ (ICV) induced memory impaired rats. *J Neuroimmunol*. 2013; 254(1–2):1–9. [PubMed: 23021418]
- Schipke CG, Ohlemeyer C, Matyash M, Nolte C, Kettenmann H, Kirchhoff F. Astrocytes of the mouse neocortex express functional N-methyl-D-aspartate receptors. *FASEB J*. 2001; 15(7):1270–1272. [PubMed: 11344110]

- Sokolova V, Ludwig AK, Hornung S, Rotan O, Horn PA, Epple M, Giebel B. Characterisation of exosomes derived from human cells by nanoparticle tracking analysis and scanning electron microscopy. *Colloids Surf B Biointerfaces*. 2011; 87(1):146–150. [PubMed: 21640565]
- Soni KB, Kuttan R. Effect of oral curcumin administration on serum peroxides and cholesterol levels in human volunteers. *Indian J Physiol Pharmacol*. 1992; 36(4):273–275. [PubMed: 1291482]
- Strimpakos AS, Sharma RA. Curcumin: preventive and therapeutic properties in laboratory studies and clinical trials. *Antioxid Redox Signal*. 2008; 10(3):511–545. [PubMed: 18370854]
- Sun D, Zhuang X, Xiang X, Liu Y, Zhang S, Liu C, Barnes S, Grizzle W, Miller D, Zhang HG. A novel nanoparticle drug delivery system: the anti-inflammatory activity of curcumin is enhanced when encapsulated in exosomes. *Mol Ther*. 2010; 18(9):1606–1614. [PubMed: 20571541]
- Thiyagarajan M, Sharma SS. Neuroprotective effect of curcumin in middle cerebral artery occlusion induced focal cerebral ischemia in rats. *Life Sci*. 2004; 74(8):969–985. [PubMed: 14672754]
- Tota S, Kamat PK, Saxena G, Hanif K, Najmi AK, Nath C. Central angiotensin converting enzyme facilitates memory impairment in intracerebroventricular streptozotocin treated rats. *Behav Brain Res*. 2012; 226(1):317–330. [PubMed: 21864581]
- Wang H, Li Y, Jiang N, Chen X, Zhang Y, Zhang K, Wang T, Hao Y, Ma L, Zhao C, Wang Y, Sun T, Yu J. Protective effect of oxysphoridine on cerebral ischemia/reperfusion injury in mice. *Neural Regen Res*. 2013; 8(15):1349–1359. [PubMed: 25206429]
- Wang S, Chen P, Zhang L, Yang C, Zhai G. Formulation and evaluation of microemulsion-based in situ ion-sensitive gelling systems for intranasal administration of curcumin. *Journal of drug targeting*. 2012; 20(10):831–840. [PubMed: 22934854]
- Wong R. NMDA receptors expressed in oligodendrocytes. *Bioessays*. 2006; 28(5):460–464. [PubMed: 16615088]
- Xin H, Li Y, Buller B, Katakowski M, Zhang Y, Wang X, Shang X, Zhang ZG, Chopp M. Exosome-mediated transfer of miR-133b from multipotent mesenchymal stromal cells to neural cells contributes to neurite outgrowth. *Stem Cells*. 2012; 30(7):1556–1564. [PubMed: 22605481]
- Xin H, Li Y, Cui Y, Yang JJ, Zhang ZG, Chopp M. Systemic administration of exosomes released from mesenchymal stromal cells promote functional recovery and neurovascular plasticity after stroke in rats. *J Cereb Blood Flow Metab*. 2013; 33(11):1711–1715. [PubMed: 23963371]
- Zhang HG, Grizzle WE. Exosomes: a novel pathway of local and distant intercellular communication that facilitates the growth and metastasis of neoplastic lesions. *The American journal of pathology*. 2014; 184(1):28–41. [PubMed: 24269592]
- Zhou Y, Li HL, Zhao R, Yang LT, Dong Y, Yue X, Ma YY, Wang Z, Chen J, Cui CL, Yu AC. Astrocytes express N-methyl-D-aspartate receptor subunits in development, ischemia and post-ischemia. *Neurochem Res*. 2010; 35(12):2124–2134. [PubMed: 21116713]
- Zhuang X, Xiang X, Grizzle W, Sun D, Zhang S, Axtell RC, Ju S, Mu J, Zhang L, Steinman L, Miller D, Zhang HG. Treatment of brain inflammatory diseases by delivering exosome encapsulated anti-inflammatory drugs from the nasal region to the brain. *Mol Ther*. 2011; 19(10):1769–1779. [PubMed: 21915101]

### Highlights

- This is the important study that describes the combined therapeutic potentials of curcumin and embryonic stem cell exosomes.
- Stem cells have rejuvenating properties and curcumin possesses anti-inflammatory, anti-lipidemic and neurorestoration properties.
- The combined therapeutic units reduced ischemic injury and restored neuro-vascular unit following ischemia-reperfusion injury in mice.

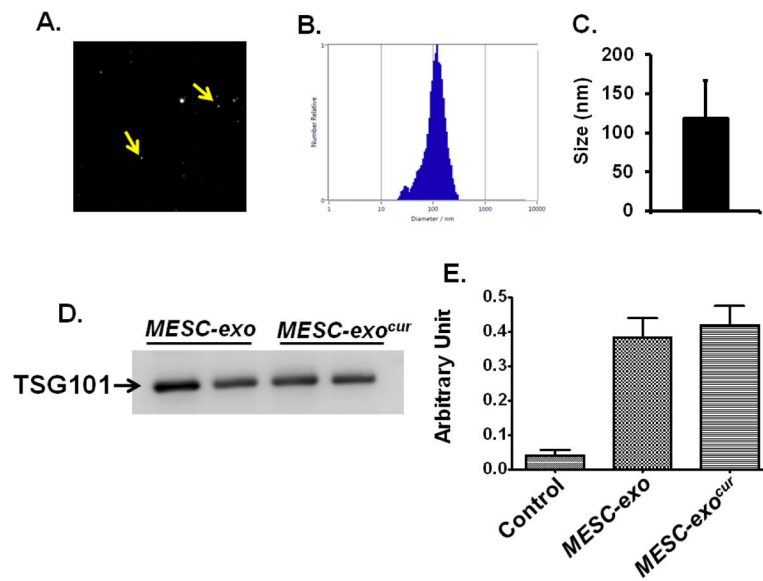


**Figure 1. Characterization of *MESC-exo<sup>cur</sup>* nano-formulation**

(A) Nano-tracking analysis image generated on the basis of Brownian motions of exosomes (indicated with yellow arrow). (B) Size distribution of *MESC-exo* through nano-tracking analysis. (C) Bar diagram representing nano-vesicle size that appeared to be  $118.0 \pm 49.8$  (mean  $\pm$  SD). (D) Western blot image representing the presence of Tumor susceptibility gene 101 (TSG101), an exosome marker, in different *MESC-exo* and *MESC-exo<sup>cur</sup>* preparations. (E) Bar graph showing acetylcholinesterase activity in *MESC-exo*, *MESC-exo<sup>cur</sup>*, and control (supernatant deprived of exosomes).

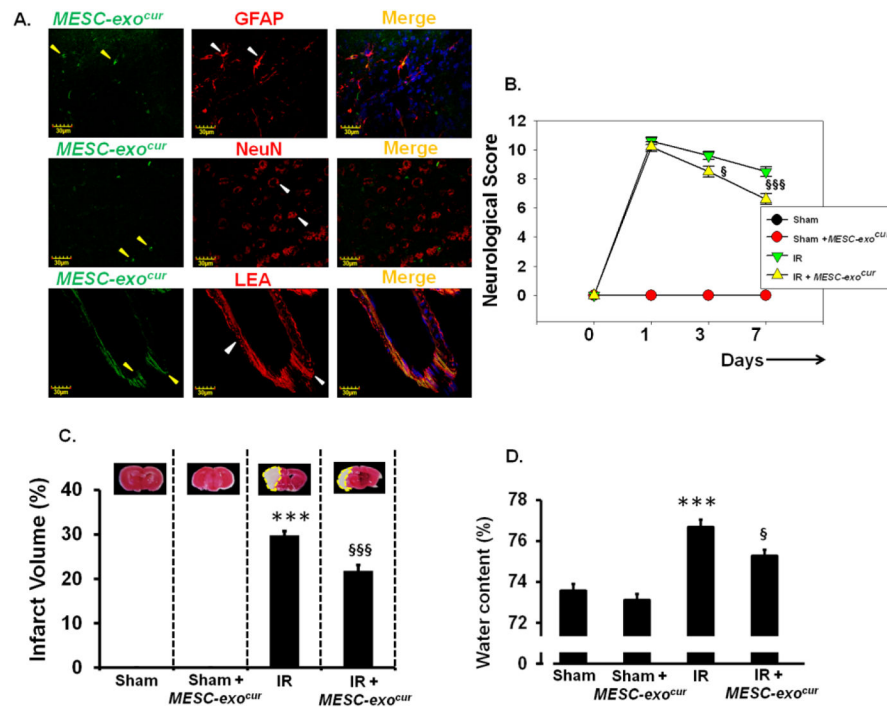


**Figure 2. Acquisition of *MESC-exo<sup>cur</sup>* by astrocytes, neurons and brain vessels, administered through intranasal route, and the effect of *MESC-exo<sup>cur</sup>* administration on neurological score, infarct volume and water content following IR-injury**

(A) Immunohistochemistry images showing the presence of fluorescently labeled exosomes (left lanes, green color, yellow arrows) in brain cortical areas. Astrocytes, neurons and brain pial vessels were stained with GFAP (top horizontal panel), NeuN (middle horizontal panel) and lycopersicon esculentum agglutinin (lower horizontal panel) respectively. Nuclei were stained with DapI (blue) and shown in merged images (right most lanes). (B) Neurological score was determined in different experimental groups at 1<sup>st</sup>, 3<sup>rd</sup>, and 7<sup>th</sup> day post-IR injury. (C) Images of tetrazolium chloride stained brain coronal sections that represent infarct volumes (pale white region) (n=8/group). The analysis of infarct volume is shown as bar diagram. (D) Bar graph showing brain water content that represents edema (n=7/group). \*\*\*p<0.001 -vs. sham, sham+MESC-exo<sup>cur</sup>, §p<0.05, §§§p<0.001 -vs. IR.

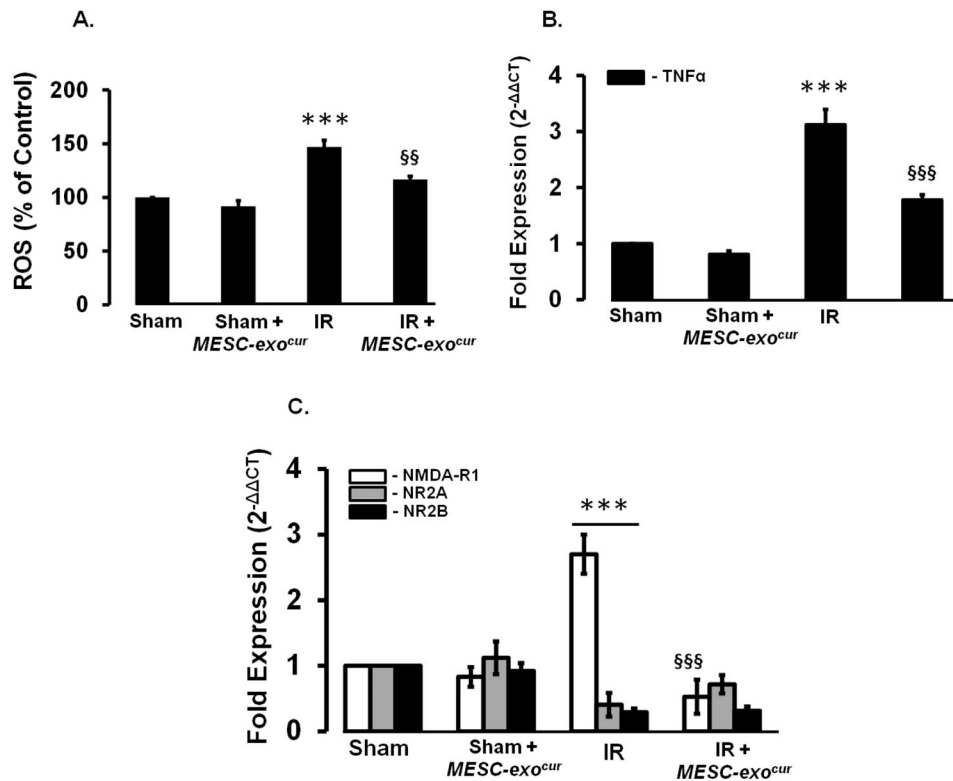


**Figure 3. *MESC-exo<sup>cur</sup>* administration decreased ROS, TNF- $\alpha$  and NMDAR1 expression**  
**(A)** Bar diagram presenting the levels of reactive oxygen species in different experimental mice brain tissues (n=6). **(B)** Bar graph showing qPCR analysis for pro-inflammatory cytokines Tumor necrosis factor-alpha (TNF- $\alpha$ ) in different experimental mice brains (n=4/group). **(C)** QPCR analysis results, represented as bar diagram, showing expressions of N-methyl-D-aspartate receptors (NR1, NR2A, and NR2B) in different experimental mice brains (n=3/group). \*\*\*p<0.001 -vs. sham, sham+MESC-exo<sup>cur</sup>, §§p<0.01, §§§p<0.001 -vs. IR.

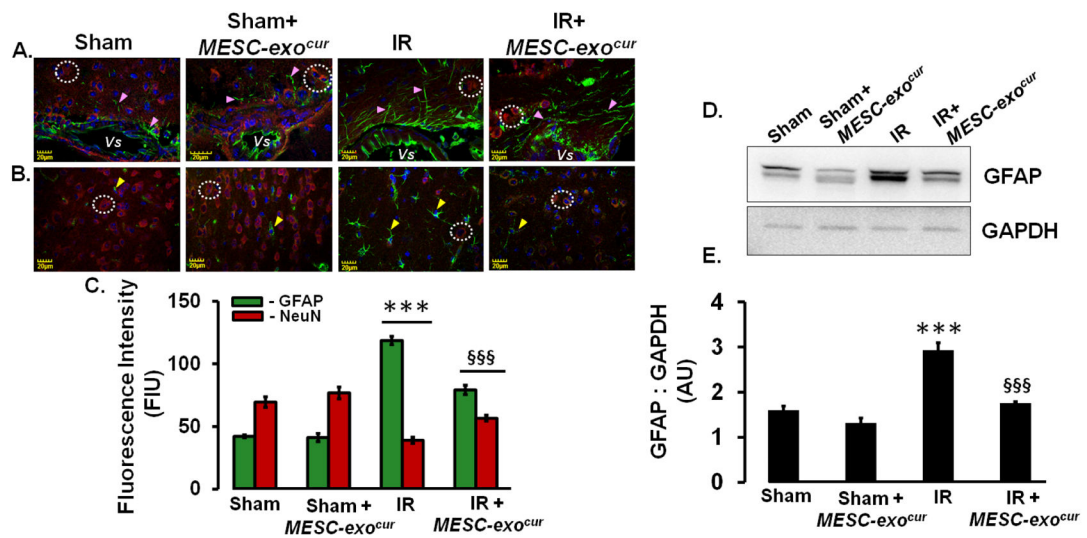


**Figure 4. *MESC-exo<sup>cur</sup>* administration reduced GFAP expression and restored NeuN positive neurons**

(A) Immunohistochemistry images showing Glial fibrillary acidic protein (GFAP, green color, pink arrowheads), neuronal nuclei positive neurons (NeuN, red color, white dotted circles) around cerebral vessels (represented as *Vs*). (B) The quantitation of GFAP stained astrocytes and NeuN positive neurons was also performed in cortical areas in different mice brains. (C) Bar diagram showing quantitative analysis for the GFAP and NeuN in different groups of the mice brains (n=6/group). (D) Representative western blot images showing GFAP and GAPDH expressions in experimental mice brain homogenates. (E) Bar graph showing densitometry analysis for GFAP band in different mice groups. Each band density was normalized with corresponding GAPDH band density (n=3/group). \*\*\*p<0.001 -vs. sham, sham+MESC-exo<sup>cur</sup>, §§§p<0.001 -vs. IR.

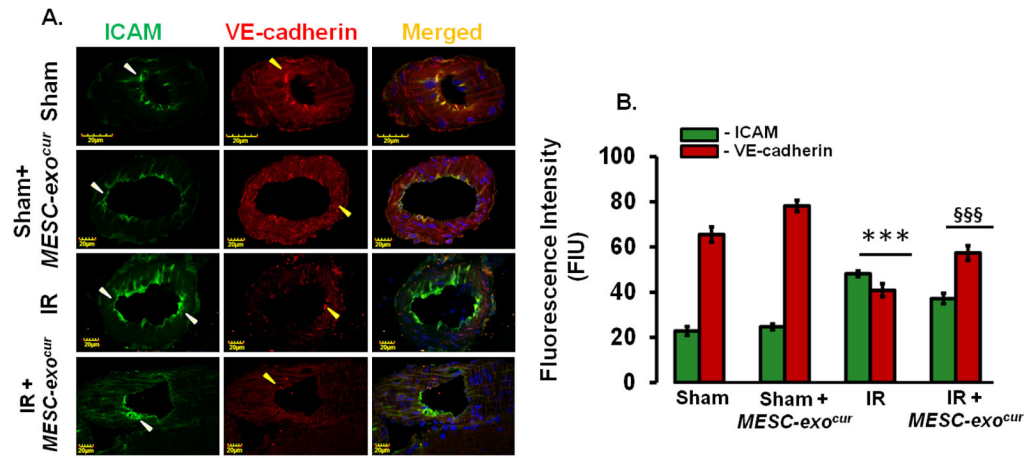


**Figure 5. *MESC-exo<sup>cur</sup>* reduced vascular inflammation and improved vascular endothelial adherent junction protein**

(A) Confocal images showing intercellular adhesion molecule-1 (left lanes, green color) and adherens junction VE-cadherin (middle lanes, red color) expressions in pial vessels of different mice groups. Merged images are shown at rightmost lane. (B) Bar graph showing analysis for ICAM and VE-cadherin expressions (n=4/group). \*\*\*p<0.001 -vs. sham, sham +MESC-exo<sup>cur</sup>, §§§p<0.001 -vs. IR.

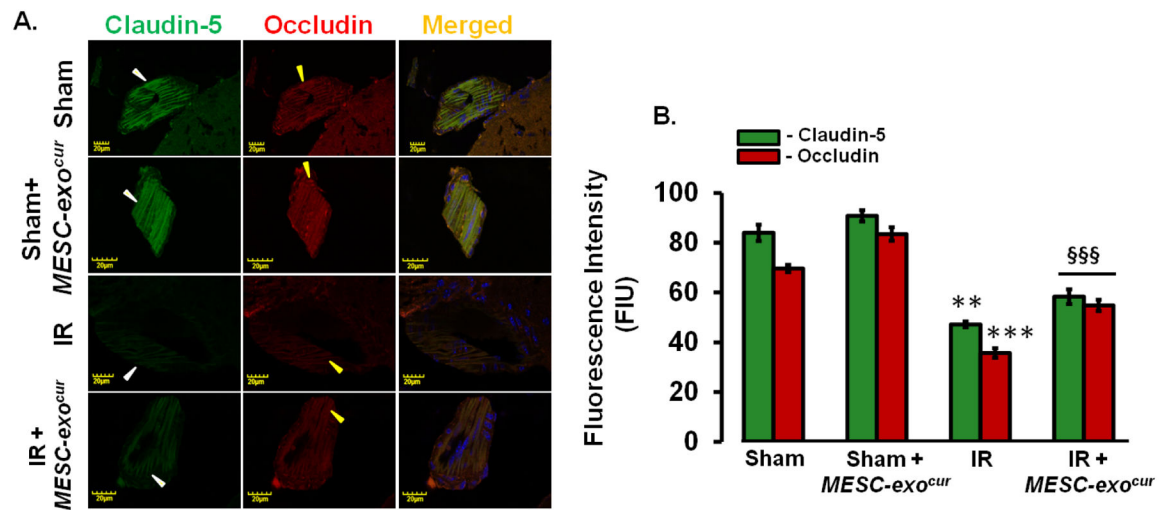


**Figure 6. *MESC-exo<sup>cur</sup>* restored vascular endothelial tight junction proteins**

(C) Confocal images of tight junction proteins, claudin-5 (left lanes, green color) and occludin (middle lanes, red color) in pial vessels of different mice brains. (D) Bar graph showing analysis of claudin-5 and occludin fluorescence intensities (n=4/group). \*\*p<0.01, \*\*\*p<0.001 -vs. sham, sham+MESC-exo<sup>cur</sup>, §§§p<0.001 -vs. IR.

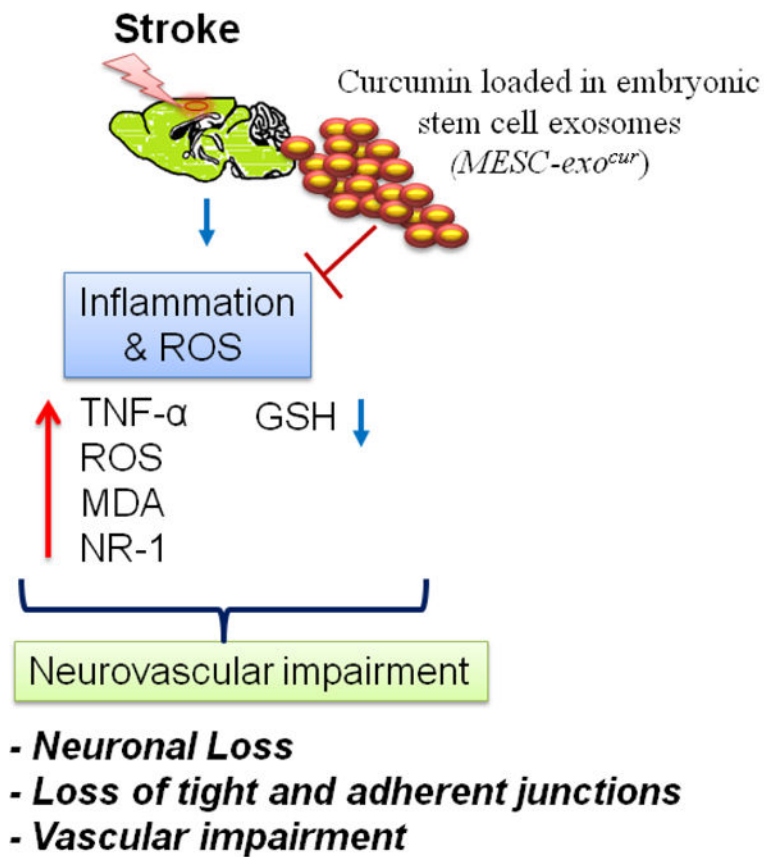


**Figure 7.** Figure representing the proposed hypothesis for the therapeutic efficacy of nano-formulation *MESC-exo<sup>cur</sup>*

*MESC-exo<sup>cur</sup>* nano-units restored neurovascular integrity in IR-injured mice by reducing inflammation and ROS levels.

**Table 1**

Malondialdehyde (MDA) and Glutathione (GSH) levels in cerebral cortex and hippocampus regions of the experimental mice brain

<b>Cerebral Cortex</b>	<b>Sham</b>	<b>Sham+ <i>MESC-exo<sup>cur</sup></i></b>	<b>IR</b>	<b>IR + <i>MESC-exo<sup>cur</sup></i></b>
MDA (nmol/mg protein)	46.2 ± 4.2	43.9 ± 5.3	302 ± 6.2	134 ± 20.3
GSH (µg/mg protein)	72 ± 8.8	65 ± 5.3	24 ± 5.9	37 ± 24

<b>Hippocampus</b>	<b>Sham</b>	<b>Sham+ <i>MESC-exo<sup>cur</sup></i></b>	<b>IR</b>	<b>IR + <i>MESC-exo<sup>cur</sup></i></b>
MDA (nmol/mg protein)	53 ± 3.8	49.9 ± 2.1	365 ± 9.2	122.5 ± 12.6
GSH (µg/mg protein)	59.4 ± 6.6	67 ± 10.8	35 ± 4.0	44 ± 2.8

Data is given as mean ± SE for each group (n=2).